Green Chemistry

Cutting-edge research for a greener sustainable future

Accepted Manuscript

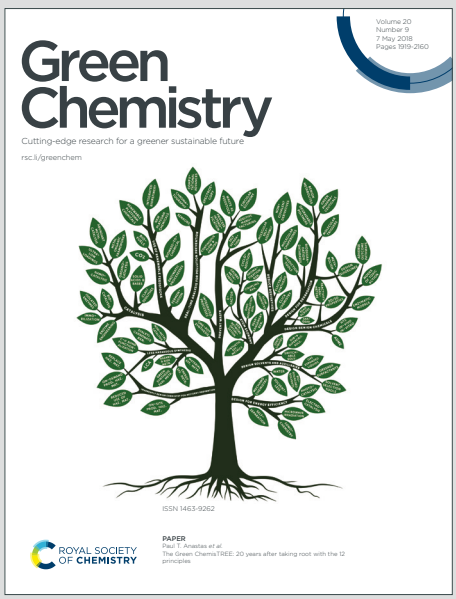

ROYAL SOCIETY OF CHEMISTRY

rsc.li/greenchem

ROYAL SOCIETY OF CHEMISTRY
View Article Online
DOI: 10.1039/D0GC01742F

Journal Name

ARTICLE

Environmentally friendly luminescent solar concentrators based on optically efficient and stable green fluorescent protein

Received 00th January 20xx,
Accepted 00th January 20xx

DOI: 10.1039/x0xx00000x

www.rsc.org/

Carlota P. A. Carlos,[1,2] Sandra F. H. Correia,[1] Margarida Martins,[3] Oleksandr A. Savchuk,[2] João A. P. Coutinho,[3] Paulo S. André,[4] Jana B. Nieder,[2] Sónia P. M. Ventura,[3] Rute A. S. Ferreira[1]*

Luminescent solar concentrators (LSCs) are a solution to overcome the mismatch between solar cells absorption and the solar spectrum, facilitating the integration of photovoltaic (PV) devices into the urban environment, since they can be incorporated in building façades and windows. Challenges include the search for environmentally friendly materials with chemical and optical stability. To overcome these drawbacks, in this work, the enhanced Green Fluorescent Protein (eGFP) was efficiently applied as an optically-active center. eGFP absorbs in the UV/visible spectra and convert it into green emission with a maximum absolute quantum yield of ~0.50. Here, we report the use of eGFP to fabricate planar LSCs in liquid (aqueous solution) and solid state (incorporated in organic-inorganic hybrids), which were coupled to commercial Si-based PV cells yielding power conversion efficiency (PCE) values up to ~0.35%, which is ~30% higher than those reported so far. These results are presented as higher than the figures of merit for naturally-based fluorescent proteins in aqueous medium, with the advantage of presenting enhanced photostability when stored at ambient conditions. Those are relevant features, uncommon in organic-based materials, that significantly contribute to the potential of naturally-based molecules in the development of LSCs as reliable, sustainable and competitive energy systems.

Introduction

The transition from the current energy matrix towards a more environmentally friendly, while affordable, is a crucial challenge of the 21st century, in which fully energetically sustainable architecture is a strategic focus through the realization of the so-called net-zero energy buildings. Hence, new technologies that integrate solar-harvesting devices into existing and new buildings are of growing relevance. Emphasis is given to planar luminescent solar concentrators (p-LSCs),[1, 2] consisting of a transparent substrate with incorporated optically-active centers able to absorb sunlight and downshift it to longer wavelengths overlapping the PV cells absorption.[1, 3] Previous studies reported that LSC operation has analogous performance under direct or diffuse light incidence,[4, 5] making LSC supported PVs less affected by shadowing of the device that typically cause efficiency losses in single-mounted PV cells, therefore allowing the use of these devices under cloudy conditions. Additionally, LSC devices can be produced with tailored shape, colour, flexibility and transparency,[6-8] which gives this technology high design freedom. LSCs can be embedded in façades or windows,[9, 10] noise barriers alongside roadways,[11-13] and integrated in wearable fabrics and outdoor furniture,[14] yielding power values up to 10 W.[15]

The selection of the right materials for LSC performance optimization is still a challenge and several types of optically active centers have been tested for this purpose,[16, 17] including organic dyes, quantum dots (QDs), lanthanide ions and metal halide clusters.[18]. Recently, a sustainable approach based on organic molecules extracted from renewable and natural sources has been followed.[19-26] Nonetheless, the low photostability of naturally-based molecules is a concern,[27, 28] since it is translated into performance deterioration of these LSCs over time.

In order to find a naturally-based optically-active center with enhanced photostability, the green fluorescent protein (GFP) was focused.[29, 30] GFP is naturally expressed in jellyfish *Aequorea victoria*[30], although usually produced by *Escherichia coli* (*E. coli*), the most common heterologous system for protein expression.[31] Recombinant GFP, usually known as enhanced GFP (eGFP), has interesting properties such as its unique spontaneous and natural emission of green light fluorescence, when excited by UV radiation,[32] which is useful in real-time imaging applications. In addition, this protein has been commonly used in molecular biology, medicine, and cell biology as a biological marker for gene expression and tracking of analyses within living cells or organelles.[33-36] Contrarily to what

[1]*Phantom-G, Department of Physics and CICECO – Aveiro Institute of Materials, University of Aveiro, 3810-193 Aveiro, Portugal. *e-mail address: rferreira@ua.pt*
[2]*Department of Nanophotonics, Ultrafast Bio- and Nanophotonics group, INL - International Iberian Nanotechnology Laboratory, Av. Mestre José Veiga s/n, 4715-330, Braga, Portugal.*
[3]*Department of Chemistry and CICECO – Aveiro Institute of Materials, University of Aveiro, 3810-193 Aveiro, Portugal*
[4]*Department of Electrical and Computer Engineering and Instituto de Telecomunicações, Instituto Superior Técnico, Universidade de Lisboa, 1049-001 Lisbon, Portugal*

†Electronic Supplementary Information (ESI) available: Detailed auxiliary data for the analysis of this work. See DOI: 10.1039/x0xx00000x

is reported for R-phycoerythrin (R-PE), which is only stable at pH 4-10 and temperatures up to 40 °C,[37] eGFP has been recognized for its much higher stability towards denaturing conditions, such as temperature, pH, and presence of proteases, organic solvents, detergents, or chaotropic agents.[29, 30] In what concerns its photoluminescence, despite analogous photo-destruction quantum yields of ~10^{-5} are found for R-PE[38] and eGFP,[39] the latter one is much more efficient with absolute emission quantum yield (q) values up to 0.66.[40]

In this work, different concentrations (from 1.4×10^{-5} to 5.5×10^{-5} M) of eGFP in aqueous solution, with high molar brightness (B) values (~5×10^{3} $M^{-1}\cdot cm^{-1}$) were used to fabricate p-LSCs based on a glass container filled with such solutions (Fig. 1), and in a bulk LSC based on a di-ureasil organic-inorganic hybrid, d-U(600), doped with eGFP. The d-U(600) is formed of polyether chains covalently bond though urea bridges to a siliceous-based network (Fig. S1). The η_{opt} values were estimated according to Eq. 1 (see experimental section for details), yielding values of ~3.3% and ~3.7% for the device based on the glass container with eGFP aqueous solutions and for the bulk LSC based on d-U(600) doped with eGFP, respectively. Moreover, the Si-based PV cells coupled to these p-LSCs yielded maximum PCE values of ~0.35% (eGFP solution) without any evidence of photo-induced degradation. These results validate the potential of eGFP for the development of stable natural-based LSCs meeting the requirements of reliable, sustainable and competitive energy systems, allowing for instance, their application in net zero energy building constructions. This approach may help in the reduction of the environmental impact relative to the state of the art by acting in three aspects: (i) the use of LSCs will allow the integration of PV devices into windows, making buildings more energy-efficient, by adding a new way to use the incident solar irradiation (without replacing the conventional use of PV cells on rooftops); and (ii) the reduction of the area of PV material needed, since they are able to concentrate sunlight in a smaller area iii) the use of nature-based optically active centers dispersed in aqueous media provide no harm to the environment during and after use, which is a relevant feature when compared to other types of state-of-the-art optically active centers (e.g. QDs, which present toxicity issues in the processing and disposing)[41, 42]. Moreover, the sustainability of the devices is also benefiting from the environmentally friendly nature of extraction and purification processes applied on the recovery of eGFP. Although the eGFP-based LSCs would be coupled to standard solar cells, we note the positive environmental impact as the solar cell will produce more energy in the presence of the LSC, when compared with bare cells.

Experimental

Materials

The Jeffamine® ED-600 (97%, Huntsman), 3-isocyanatopropyl triethoxysilane (ICPTES, 95%, ABCR), tetrahydrofuran (THF, 99%, Sigma-Aldrich) were used as purchased. The microorganism *E. coli* BL21(DE3) pLysS genetically modified to carry the plasmid pET-28(a) to express the recombinant eGFP was kindly provided by the Molecular and Cellular Biology Laboratory of the School of Pharmaceutical Sciences from Universidade Estadual Paulista "Júlio de Mesquita Filho". The components of Luria-Bertani culture media, namely tryptone and yeast extract, were purchased from Oxoid, while NaCl was acquired from Panreac. The antibiotics used in cell culture, kanamycin disulfate salt from Streptomyces kanamyceticus and chloramphenicol (> 98 wt%), were supplied by Sigma as well as the isopropyl β-d-1-thiogalactopyranoside (IPTG, > 99 wt%). The components of the Tris-HCl buffer, namely tris(hydroxymethyl)aminomethane and chloridric acid (37%), were acquired from Pronalab and Sigma-Aldrich, respectively.

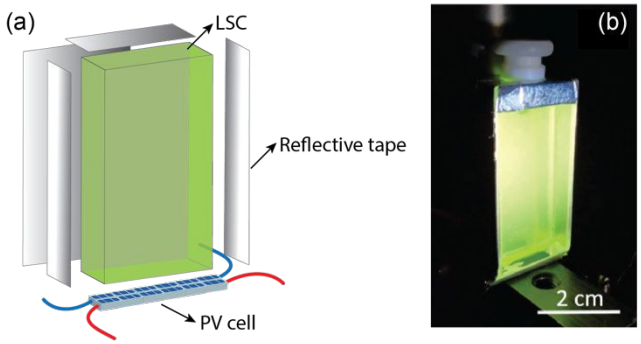

Fig. 1 (a) Schematic representation of the p-LSCs and (b) photograph of the p-LSC based on a glass container filled with eGFP with concentration of 5.5×10^{-5} M, under AM1.5G illumination. The PV cell is located at the bottom edge.

Cell cultivation for eGFP production and extraction

The methodologies previously reported for the cell cultivation, eGFP production and eGFP extraction were here adopted.[35] In the end of the extraction step, the supernatant obtained and containing the fluorescent protein was diluted in different concentrations to be used as an optically active layer for LSC applications. The eGFP concentration was measured using a calibration curve by the fluorescence intensity in the maximum of the variant used (excitation at 485 nm and emission at 530 nm) in a microplate reader (Synergy HT microplate reader – BioTek). The sample of pure eGFP was obtained using a methodology previously established.[43] A raw extract was purified using an aqueous biphasic system composed of 45% of propylene glycol 400, 12% of cholinium chloride, 10% of eGFP extract, and 33% of ultrapure water. The system was homogenized and centrifuged at 1500 xg, 5 min at 4°C. The phases were separated, and the eGFP-rich phase was submitted to ultrafiltration several times using centrifugal concentrators Vivaspin®20 until all phase components are removed.

Synthesis of the eGFP-doped hybrid monolith

1.0 mL (1.67 mmol) of Jeffamine® ED-600 and 0.5 mL of THF were mixed and stirred at room temperature to get a transparent solution. Then, 0.90 mL (3.42 mmol) of ICPTES was added dropwise under stirring with the molar ratio of ED-600:ICPTES=1:2. The obtained sol was stirred at room temperature for further 2 h. After, 0.5 mL of eGFP solution

View Article Online
DOI: 10.1039/D0GC01743F

(5.5×10^{-5} M) was added to the above-mentioned sol. The resulting mixture was stirred for 15 minutes and placed at ambient atmosphere. The gelation occurred within two days and the resultant gel dried at room temperature. The molecular density of eGFP in the hybrid host was calculated based on the premises that all the solvent (added or produced over the sol–gel condensation) evaporated after the processing and the density of the resulting hybrid monolith was ~1.0 $g.cm^{-3}$, approximating the molecular eGFP concentration in the monolith to that of the incorporated solution.

UV/Visible Absorption

UV/visible absorption spectra were measured using a Lambda 950 dual-beam spectrometer (Perkin-Elmer).

Photoluminescence Spectroscopy

The room-temperature photoluminescence spectra were recorded with a modular double-grating excitation spectrofluorimeter with a TRIAX 320 emission monochromator (Fluorolog-3, Horiba Scientific) and a spectrofluorimeter (FluoroMax-4, Horiba Scientific) equipped with a monochromator, both coupled to a R928 Hamamatsu photomultiplier. Emission decay curves were recorded at room temperature on a Fluorolog TCSPC spectrofluorometer (Horiba Scientific) coupled to a TBX-04 photomultiplier tube module (950 V) and a 200×10^{-9} s time-to-amplitude converter with a delay of 70×10^{-9} s (Supporting Information for details). The exciting source was a Horiba/Jobin–Yvon pulsed diode (NanoLED-390, peak at 388 nm, 1.2×10^{-9} s pulse duration, 1 MHz repetition rate, and 150×10^{-9} s synchronization delay). Due to the novelty of the fabricated eGFP-doped hybrid material, emission and excitation spectra were recorded for various excitation and detection wavelengths at room temperature and at low temperatures of 13 K, respectively (Fig. S4 and S5) for a better assessment of interaction between the eGPF and host matrix, namely energy transfer between the organic-inorganic host matrix excited states to the eGFP chromophore.

Absolute Emission Quantum Yield

The *q* values were measured at room temperature using a system (Quantaurus-QY Plus C13534, Hamamatsu) with a 150 W xenon lamp coupled to a monochromator for wavelength discrimination, an integrating sphere as the sample chamber, and a multichannel analyzer for signal detection. The method is accurate to within 10%. The *q* values were measured for the as-prepared sample and the measurement was repeated after 12 months with the sample being kept under ambient conditions and after exposition to AM1.5G irradiation for LSC characterization. The *q* values are analogous, demonstrating the optical stability of the prepared eGPF-based LSCs.

Streak Camera Imaging

Streak camera images were recorded using a Streak imaging setup, with a picosecond pulsed diode laser (467 nm laser with ~69 pulse duration (M10306-27 and controller PLP10, Hamamatsu), a delay unit (C1097-05, Hamamatsu) and the general streak camera (C90001, Hamamatsu), equipped with the slow sweep unit (M10913, Hamamatsu) and a 2D charged-coupled-device (CCD) camera (Orca-R2, Hamamatsu), controlled by the HPA-TA software (Hamamatsu). The pulsed excitation is guided to the sample and photoluminescence collected in a 90-degree configuration. After passing a long pass filter (473LP nm, AHF Analysentechnik,) the signal is focussed on the Czerny–Turner spectrograph (Acton SP2300, Princeton Instruments, gratings with $150 g.mm^{-1}$) located in front of the Steak unit. The HPA-TA tau software (Hamamatsu) was used for data analysis.

Optical Conversion Efficiency (η_{opt}), External Quantum Efficiency (EQE) and Power Conversion Efficiency (PCE)

The η_{opt} was calculated in this work following literature[44] as described in Eq. 1:

$$\eta_{opt} = \frac{P_{out}}{P_{in}} = \frac{I_{SC}^{L} V_0^{L} A_e \eta_{solar}}{I_{SC} V_0 A_s \ \eta_{PV}} \quad (1)$$

where I_{SC}^{L} and V_0^{L} represent the short-circuit current and the open voltage when the PV device is coupled to the LSC, Fig. 1 (I_{sc} and V_0 are the corresponding values of the PV device exposed directly to the solar radiation), A_s and A_e are the exposed and total edge area respectively, η_{solar} is the efficiency of the PV device relatively to the total solar spectrum and η_{PV} is the efficiency of the PV device at the LSC emission wavelengths. Three measurements were performed for each case, with a relative error ($\eta_{opt}/\Delta\eta_{opt}$) below 10%. The experimental η_{opt} values were determined by illuminating the top surface of the LSCs with simulated AM1.5G illumination. The optical power at the LSC output was estimated using a commercial c-Si PV cell (KXOB22-01X8F, IXYS) coupled to one edge of the LSC, while the other edges were covered with reflective tape (Fig. S2) to reduce the losses by directing all emitted photons to the photovoltaic cell. This method should deliver similar results as in the case of having photovoltaic cells coupled to all the edges of LSCs (Fig. S3). The I_{sc} and V_0 values were measured using a source meter device (2400 SourceMeter SMU Instruments, Keithley). All measurements were performed in real-life conditions, under AM1.5G illumination (1000 $W.m^{-2}$) using a 150 W xenon arc lamp, class A, solar simulator (Model 10500, Abet Technologies). The temperature increase induced by the local heating due to the exposition to the solar radiation was monitored, revealing that the maximum temperature increase reaches 35 °C, which did not influenced the performance of the LSCs. The mismatch in the UV spectral region between the AM1.5G solar irradiance and that of the Xe lamp in the solar simulator was taken into consideration following a methodology reported in detail elsewhere.[45] The PCE was calculated as follows:

$$PCE = \frac{P_{out}^{el}}{P_{in}} = \frac{I_{SC}^{L} V_0^{L} FF}{A_S \int_{\lambda_1}^{\lambda_2} I_{AM1.5G}(\lambda) d\lambda} \quad (2)$$

where P_{out}^{el} and FF=0.75 are the PV device output electrical power and fill factor of the PV cell, respectively.
The EQE was calculated by applying Eq. 3:

$$EQE(\lambda) = \frac{I_{SC} \cdot h \cdot c}{P_{in} \cdot e \cdot \lambda} \quad (3)$$

where e is the charge of the electron, h is the Planck's constant, c is the speed of light and λ is the wavelength. The solar simulator was coupled to a monochromator (Triax 180, Horiba Scientific). The I_{sc} and P_{in} values were measured using the above mentioned sourcemeter and a c-Si calibrated photodiode (FDS1010, Thorlabs), respectively.

Results and discussion

Optical characterization

The excitation spectra of the eGFP solutions (from 1.4×10^{-5} to 5.5×10^{-5} M) presented in Fig. 2(a), reveal the A (400 nm) and B (480 nm) bands related to eGFP excited states, corresponding to the neutral protonated and deprotonated form of the chromophore, respectively.[46, 47] Excitation to the neutral singlet excited state A* can initiate a fast excited state proton transfer (ESPT) to form an intermediate singlet state I*, [48, 49] which is the deprotonated chromophore in the geometry of the protonated ground state. The primary fate of I* is the decay back to the ground state through fluorescence. The absorption bands of the two anionic forms, I and B, overlap and are responsible for the absorption peak at ~488 nm seen in Fig. 2(b).

The emission spectra, also shown in Fig. 2(a), are dominated by the eGFP characteristic emission peak around 510 nm, attributed to the overlapping emission of the I and B excited states, with a shoulder at 540 nm. A supplementary weak emission at 450 nm is due to the relaxation to the ground state of the protonated form (A band), whereas the shoulder at around 287 nm is related to the aromatic region of the protein.[49] The spectral distance between the absorption and emission band maxima, *i.e.*, the Stokes-shift, reported for this solution is ~884 cm^{-1} (22 nm), which is quite small and justified by the rigidity of the chromophore environment, that minimizes the non-fluorescent relaxation to a ground state.[50] To enable processing the natural emitters as solid monoliths, the eGFP molecules were incorporated into an organic-inorganic hybrid host matrix, and the photoluminescence properties of the hybrid were additionally studied. The emission spectra are dominated by the blue-green emission attributed to electron–hole recombination occurring in the urea groups and within oxygen defects in the siliceous skeleton of the d-U(600) hybrid host (315–600 nm), and by eGFP characteristic emission.[51, 52] Focusing our attention on the eGFP-related contribution, the emission peak at 513 nm (with a shoulder at 548 nm) is rising in relative intensity as the excitation wavelength approaches the excitation maximum of eGFP around 470 nm. When compared with the emission spectra of the incorporated solution (5.5×10^{-5} M), the eGFP emission is slightly red-shifted and broader with a full-width-at-half-maximum (FWHM) of ~40 nm *versus* the ~31 nm reported for the solution. The emission broadening observed after the incorporation of eGFP in the hybrids is probably related to changes in the local structure of the protein and due to the rigidity of the host.[15] The emission spectra of the d-U(600) host is formed by a large broad band (250–400 nm), with peak position red-shifting as the excitation wavelength increases, as previously observed in ureasil organic-inorganic hybrids.[53, 54]

View Article Online
DOI: 10.1039/D0GC01742F

At room temperature, the excitation spectra are dominated by the eGFP excited states and those of the d-U(600) hybrid host. Monitoring within the eGFP emission (512 and 550 nm), one can see its characteristic excited states (A, B and I bands). When monitoring the d-U(600)-GFP hybrid (330 and 450 nm), the excitation spectra are dominated by the hybrid excited states that appear in two broad bands, 250–315 nm and 315–400 nm. As the detection wavelength increases, the host-related excitation shifts to lower energies.[55] Moreover, the excitation spectrum monitored within the host emission broad band also overlaps with that monitored within the eGFP band in the UV spectral region (from 325 to 400 nm), pointing to possible energy transfer between the hybrid excited states and eGFP.

Time dependent fluorescent behaviour was also monitored using streak-camera technology. Streak camera images were recorded for the eGFP solutions and for the eGFP-doped organic-inorganic hybrid. The images recorded for the different solutions are very similar, with an emission maximum at 510 nm and a shoulder at 540 nm, both characteristic of the eGFP emission, Fig. 2(c-f) and S5. The images shown in Fig. 2(c-f) correspond to that of the more concentrated solution (5.5×10^{-5} M), as it was the one incorporated in the hybrid host, and to that of the eGFP-doped d-U(600) hybrid monolith, for direct comparison. Qualitatively, one can see that the emission is more intense around 510 nm (red area) for both the solution and the organic-inorganic hybrid. The signal-to-noise ratio is much lower in the streak image recorded for eGFP-doped d-U(600) due to the lower intensity of eGFP emission, justified by the decrease in the number of eGFP optical active centres per unit volume. The emission band is, however, very similar in the two samples in terms of spectral range and temporal decay (<15 ns).

Fluorescence decay curves were integrated over the full wavelength range (460–560 nm)[56] of each image and the fluorescence lifetime values were calculated resorting to a two exponential decay model, due to simultaneous excitation of the two distinct fluorescent states B and I, responsible for the radiative deactivation of eGFP at around 510 nm. The lifetimes resulting from the data best fitting for the three solutions and the organic-inorganic hybrid (Table 1) are in agreement with those reported in literature for the I and B excited states, τ_I~3 and τ_B~2 ns respectively.[49, 57] The ESPT process from A* to I* was also investigated, through time-correlated single photon counting, monitoring the eGFP fluorescence over time of the eGFP solutions at 510 nm when exciting within the A band, at 390 nm. For all three solutions, the experimental curves are well described by single exponential functions (Fig. S7), yielding lifetime values similar to those previously reported in literature for the fluorescence decay of the I band, τ_1~3 ns, although slightly higher (~0.3-0.4 ns) than those reported previously, when the excitation wavelength was within the I band of eGFP (467 nm). The emission properties were further quantified through the measurement of the q values (Table 2). A maximum q is observed for all eGFP-based samples under488 nm excitation (the excitation maxima of eGFP), to which we may

View Article Online
DOI: 10.1039/D0GC01742F

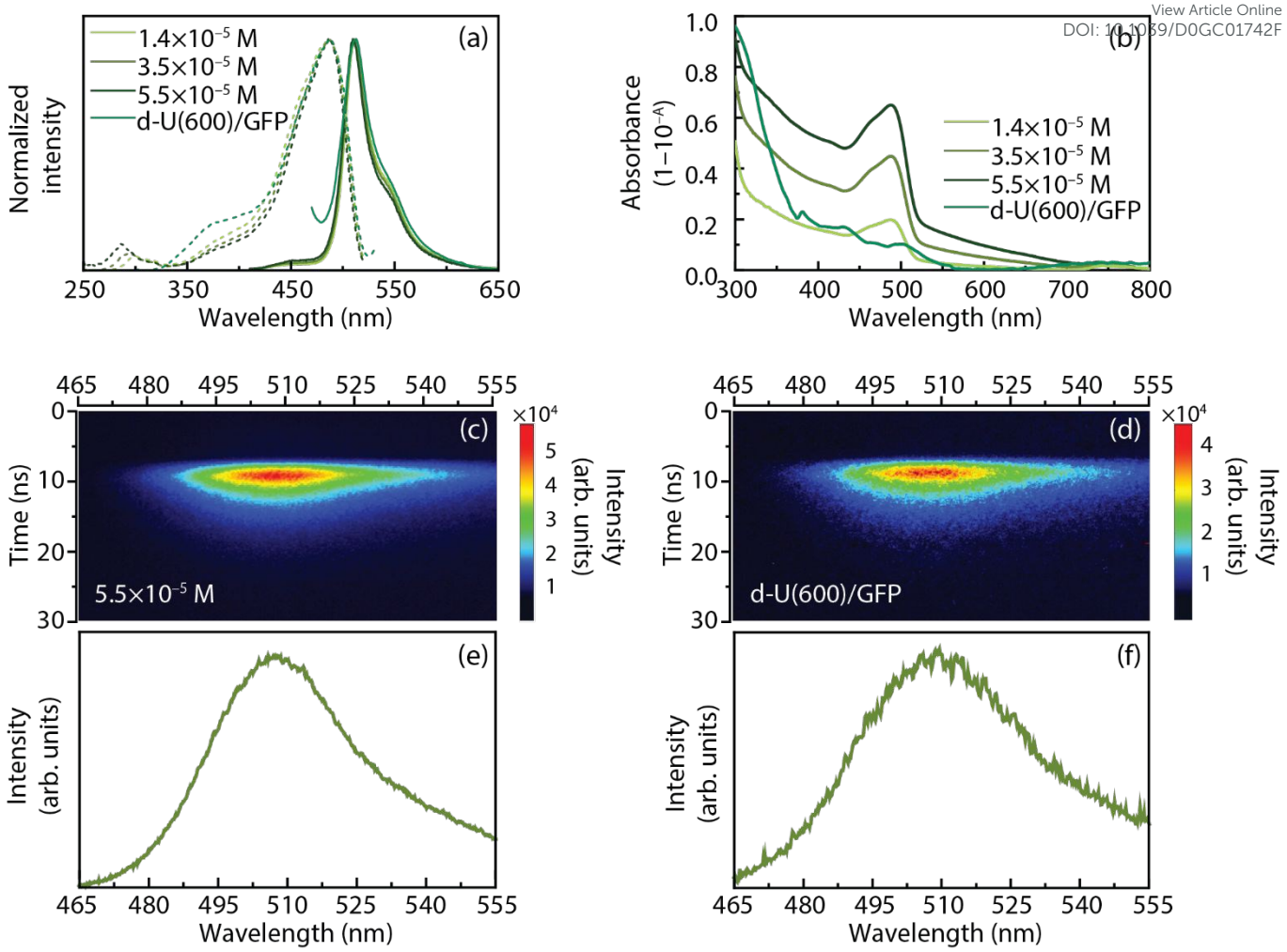

Fig. 2 (a) Emission (solid lines) and excitation spectra (dashed lines) of the eGFP aqueous solutions and doped d-U(600) monolith, excited at 390

View Article Online
DOI: 10.1039/D0GC01742F

and 365 nm and monitored at 543 and 550 nm, respectively. (b) Absolute absorbance of eGFP aqueous solutions and doped hybrid. Streak image of the (c) eGFP in solution and (d) of the hybrid sample (respective intensity colour bar next to each figure). The respective integrated fluorescence emission spectra, (e) and (f), are shown on the bottom.

Table 1. Emission lifetime values (τ), calculated from the best fit to the decay curves measured for the eGFP solutions when exciting in the A band (390 nm) and, simultaneously, in the B and I excited states (467 nm) of the protein, as a function of eGFP concentration.

		467 nm	390 nm
	(×10^{-5}) [M]	τ_B/τ_I [ns]	τ_I [ns]
eGFP aqueous solutions	1.4	1.9±0.1/3.08±0.05	3.4±0.1
	3.5	1.8±0.3/3.02±0.03	3.3±0.1
	5.5	1.5±0.3/2.97±0.04	3.4±0.1
eGFP-doped d-U(600)	5.5	1.6±0.1/3.2±0.3	—

find a nearly constant value for the tested solutions, with an average value of 0.51±0.05. The eGFP-doped hybrid q values were measured along the eGFP excitation range from 360–500 nm (Table S1) and is found to increase towards the excitation maximum of eGFP (470-500 nm), with a constant q value of 0.33±0.03. The maximum q reported for the hybrid sample is lower than that reported for the solution with the same eGFP

concentration, indicating a quenching of the eGFP emission after its incorporation into the host matrix. The *q* values are lower than those previously reported in literature of 0.80, found for eGFP in phosphate buffers for more concentrated samples (~10^{-2} M).[58]

The light-harvesting ability of all the eGFP aqueous solutions relative to the AM1.5G spectrum was studied by absorption spectroscopy. Fig. 2(b) shows the absorption spectra of the eGFP aqueous samples, which resemble the excitation spectra above mentioned, apart from the contribution of the water absorption. There are no significant spectral changes in the absorption spectra as the concentration is varied, while the absolute absorbance value increases with concentration with molar extinction coefficient values (ε) of ~10^{-4} M^{-1}.cm^{-1} (Table 2).[59] Combining emission efficiency and radiation harvesting ability, brightness values, $B=q\times\varepsilon$,[60] of ~0.5×10^4 M^{-1}·cm^{-1} (Table 2) were also calculated.

Table 2. Integral overlap (O), molar extinction coefficient (ε), absolute emission quantum yield (q) and brightness (B) as function of the eGFP concentration. The ε, *q* and *B* values refer to 488 nm.

	(×10^{-5}) [M]	*O* (×10^{20}) [photons s^{-1} m^{-2}]	ε (×10^4) [M^{-1} cm^{-1}]	*q*	*B* (×10^4) [M^{-1} cm^{-1}]
eGFP aqueous solutions	1.4	0.9	1.04	0.49±0.04	0.51
	3.5	2.2	0.93	0.52±0.05	0.49
	5.5	3.4	0.99	0.51±0.05	0.51
eGFP-doped d-U(600)	5.5	1.0	0.16	0.33±0.03	0.05

To quantify the ability of the LSCs to absorb the sunlight, the overlap integral (*O*) between the eGFP aqueous solutions absorption spectra and the solar irradiation spectra and the solar irradiation on Earth was calculated,[61] revealing that *O* increase with the concentration (Fig. 3(a) and Table 2). In particular, the 5.5×10^{-5} M eGFP aqueous solution has the potential to absorb ~8% of the solar photon flux on the Earth (4.3×10^{21} photons·s^{-1}·m^{-2}).[61] Likewise, the overlap integral *O* was calculated for the hybrid sample, Fig. 3(a), resulting in a smaller value than the ones found for the eGFP aqueous solutions. Also, ε was calculated at the eGFP absorption maximum wavelength (488 nm) for the eGFP-doped monolith, yielding the value of 1.6×10^3 M^{-1}·cm^{-1}, which leads to a *B* value of 0.5×10^3 M^{-1}·cm^{-1}. We should note that these optical features are remarkable, comparable to the ones reported for synthetic organic dyes or rare-earth complexes-based materials (Table S2) if we take into account the fact that this is an environmentally friendly approach, with no toxicity issues in what concerns processing or disposing. Meanwhile, the sustainable nature of eGFP (use as the optically active center) is also contributing to improve the biocompatible nature of the whole device, since it is obtained by sustainable water-based instead of the volatile organic solvents-based downstream processes.[43]

Fabrication of a p-LSC based on eGFP aqueous solutions and d-U(600) matrix doped with eGFP

Taking advantage of the optical properties of the eGFP aqueous solutions and the ability to harvest the AM1.5G radiation, converting it into visible emission, the solutions were used to fill a glass container and fabricate p-LSCs presented in Fig. 1(b). The LSC performance was quantified by the η_{opt} values through Eq. 1, as function of the concentration, yielding maximum η_{opt} (also known as external quantum efficiency)[62, 63] values of 3.3±0.1%. for the 5.5×10^{-5} M aqueous solution in the total incident spectral range, which is comparable to values found for other reported p-LSCs with optically active centres dispersed in liquid medium (Table 3).[64-70] The internal quantum efficiency, defined as the ratio between the photon flux reaching the PV cell and the fraction of incident photons that are absorbed by the LSC,[62, 63] was estimated to be ~19%. Also, the maximum PCE value was 0.35±0.01%, for the same solution. The EQE values were calculated for the 300–800 nm range, yielding maximum values of 3.8% (Fig. S8), with spectra showing good correlation with the excitation spectrum of the solution, Fig. 3(b).

Comparing these results with reported LSCs with optically active centres dispersed in liquid medium (Table 3), the presented PCE values are ~30% higher than those reported for a p-LSC based on R-PE fluorescent protein,[26] with the advantage of presenting enhanced photostability. Larger values were only reported for LSCs with synthetic optically active centers dispersed in non-aqueous media[64-70]. Moreover, this work showed the possibility of processing eGFP as thin films or monoliths by incorporation in an organic-inorganic hybrid matrix (Fig. S9-S11).

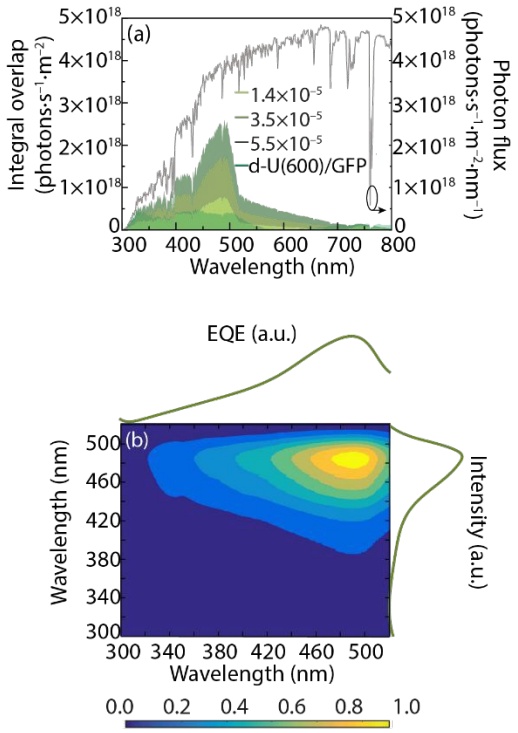

Fig. 3 (a) Integral overlap between the solar photon flux and the absolute absorbance for each one GFP-based sample. The solar photon flux on Earth at AM1.5G is also presented (right y axis). (b) Cross correlation between the EQE of the PV cell coupled to the p-LSC based on the 5.5×10^{-5} M solution and its excitation spectrum. The colour-scale intensity is a measure of the correlation.

Table 3. η_{opt} (%) and PCE (%) values for p- LSCs which optically active centres are dispersed in distinct liquid media. The concentration ([ ], M) of the active centres on the liquid media and the LSC dimensions (cm^3) are also presented.

Medium	Active centre	[ ]	Dimensions*	η_{opt}	PCE	Ref.
Water	eGFP	5.5×10^{-5}	2.0×2.0×1.0	3.3	0.35	(this work)
	R-PE	3.3×10^{-7}		6.88	0.27 (Si)	26
PPC/EG	Rhodamine B	-	2.5×7.6×0.5	15.3	-	64
	LDS698			3.6		
	LDS821	$\sim10^{-4}$		2.9		
Cl-benzene	MDMO-PPV	$\sim10^{-3}$		5.9		
	MEH-DOO-PPV	-		5.0		
	Red F	8×10^{-6}		19.8		
toluene	CdSe/ZnS	3×10^{-6}		1.6		
	CZISe/ZSe	1.4×10^{-6}	2.0×2.0×0.2	3.7	0.83	65
	CdSe/ZnS	3×10^{-6}	4.5×1.2×0.4	0.5	1.2 (Si)	66
	PbS	1.9×10^{-4}	-	12.6	3.2 (Si)	
	Lumogen F Red 300	4×10^{-3}	2.0×2.0×0.2	12.0	-	67
	Lumogen Red 305	1.2×10^{-7}	10×3.5×1.0	-	2.3 (Si)	68
TX-100	KI	-	5×10×0.28	20.2	-	69
	Sulphorhodamine 101			18.2		
	BASF-402			19.7		
	BASF-241			13.9		
LC E7	Coumarine/perylene	8×10^{-3}	5×5×nd	3.2*	-	70

Liquid crystal Nematic=LC E7, TX-100=polymer Triton X-100, PPC=Propylene carbonate, EG=ethylene glycol, Cl-bez=Chlorobenzene; $^{*}\eta_{opt}$ is simply defined as $\eta_{opt}=P_{out}/P_{in}$, without mentioning the definition behind it. **length×width×thickness; nd=not defined.

Conclusions

View Article Online
DOI: 10.1039/D0GC01742F

In this work, naturally-based LSCs based on eGFP aqueous solutions, as well as bulk ones based on an eGFP-doped organic-inorganic hybrid, were developed. These materials present a large overlap with the solar irradiance on Earth, with eGFP absorbing at 250–500 nm and converting this radiation into visible emission, around 510 nm. The best performance device was the planar LSC based on 5.5×10^{-5} M aqueous solution with η_{opt} = 3.3% and PCE values ~30% higher than the current figures of merit reported so far. Although in its infant development stage, these values and the stability of eGFP as an optically active material are a starting point for the development of sustainable and more efficient LSCs based on fluorescent proteins and may be a breakthrough for future developed nature-inspired LSCs as a cheaper and sustainable PV solution, with the potential to reduce the environmental impact in the PV integration of state-of-the-art solar cells. Moreover, this work will open the door for the exploration of other efficient bio-based compounds with reduced toxicity, costs and environmental impact, following the guidelines of Green Chemistry Principles, e.g. by selecting optically active molecules obtained through innocuous solvents like water instead of using the traditional organic solvents. In the end, this strategy will enable the design of energetically efficient materials and products, helping to approach energetically sustainable architectures.

Conflicts of interest

There are no conflicts of interest to declare.

Acknowledgements

This work was developed within the scope of the project CICECO-Aveiro Institute of Materials, (UIDB/50011/2020 & UIDP/50011/2020), Instituto de Telecomunicações (UIDB/50008/2020-UIDP/50008/2020), INL – International Iberian Nanotechnology Laboratory (CCDR-N, via project Nanotechnology Nanotechnology based functional solutions (NORTE-01-0145-FEDER-000019), Solar-Flex (CENTRO-01-0145-FEDER-030186), and SusPhotoSolutions (CENTRO-01-0145-FEDER- 000005) financed by national funds through the FCT/MEC and when appropriate co-financed by FEDER under the PT2020 Partnership through European Regional Development Fund (ERDF) in the frame of Operational Competitiveness and Internationalization Programme (POCI). L.S.F. from CICECO is gratefully acknowledged by the synthesis of the hybrid sample. M. Martins thanks FCT for the doctoral grant SFRH/BD/122220/2016.

References

1. W. H. Weber and J. Lambe, *Appl. Optics*, 1976, **15**, 2299-2300.
2. A. Goetzberger and W. Greubel, *Appl. Phys.*, 1977, **14**, 123-139.

3. R. Reisfeld and S. Neuman, *Nature*, 1978, **274**, 144-145.
4. A. Goetzberger and V. Wittwer, *Sol. Cells*, 1981, **4**, 3-23.
5. G. Lifante, F. Cusso, F. Meseguer and F. Jaque, *Appl. Optics*, 1983, **22**, 3966-3970.
6. F. Meinardi, H. McDaniel, F. Carulli, A. Colombo, K. A. Velizhanin, N. S. Makarov, R. Simonutti, V. I. Klimov and S. Brovelli, *Nat. Nanotechnol.*, 2015, **10**, 878-885.
7. Y. M. Zhao, G. A. Meek, B. G. Levine and R. R. Lunt, *Adv. Opt. Mater.*, 2014, **2**, 606-611.
8. M. G. Debije, *Adv. Funct. Mater.*, 2010, **20**, 1498-1502.
9. B. McKenna and R. C. Evans, *Adv. Mater.*, 2017, **29**, 1606491.
10. B. P. V. Heiz, Z. Pan, G. Lautenschlager, C. Sirtl, M. Kraus and L. Wondraczek, *Adv. Sci.*, 2017, **4**, 1600362.
11. M. G. Debije, C. Tzikas, M. M. de Jong, M. Kanellis and L. H. Slooff, *Renew. Energ.*, 2018, **116**, 335-343.
12. M. G. Debije, C. Tzikas, V. A. Rajkumar and M. M. de Jong, *Renew. Energ.*, 2017, **113**, 1288-1292.
13. M. Kanellis, M. M. de Jong, L. Slooff and M. G. Debije, *Renew. Energ.*, 2017, **103**, 647-652.
14. *I.-G. Lim, S.-W. Kang, C.-h. Hyoung, K.-H. Park, S.-E. Kim, T.-W. Kang, H.-I. Park, J.-H. Hwang, B.-G. Choi, T.-Y. Kang, J.-B. Kim, K.-S. Kim and M.-A. Chung*, US Pat., US20140015470 A1, 2014.
15. A. R. Frias, E. Pecoraro, S. F. H. Correia, L. M. G. Minas, A. R. Bastos, S. Garcia-Revilla, R. Balda, S. J. L. Ribeiro, P. S. Andre, L. D. Carlos and R. A. S. Ferreira, *J. Mater. Chem. A*, 2018, **6**, 8712-8723.
16. S. F. H. Correia, V. D. Bermudez, S. J. L. Ribeiro, P. S. Andre, R. A. S. Ferreira and L. D. Carlos, *J. Mater. Chem. A*, 2014, **2**, 5580-5596.
17. F. Purcell-Milton and Y. K. Gun'ko, *J. Mater. Chem.*, 2012, **22**, 16687.
18. Y. M. Zhao and R. R. Lunt, *Adv. Energy Mater.*, 2013, **3**, 1143-1148.
19. A. Dey, S. A. Moyez, M. K. Mandal and S. Roy, *Mater. Today-Proc.*, 2016, **3**, 3498-3504.
20. N. J. L. K. Davis, R. W. MacQueen, S. T. E. Jones, C. Orofino-Pena, D. Cortizo-Lacalle, R. G. D. Taylor, D. Credgington, P. J. Skabara and N. C. Greenham, *J. Mater. Chem. C*, 2017, **5**, 1952-1962.
21. T. C. Han, J. J. Zhao, T. Yuan, D. Y. Lei, B. W. Li and C. W. Qiu, 2013, **6**, 3537-3541.
22. V. Fattori, M. Melucci, L. Ferrante, M. Zambianchi, I. Manet, W. Oberhauser, G. Giambastiani, M. Frediani, G. Giachi and N. Camaioni, *Energ. Environ. Sci.*, 2011, **4**, 2849-2853.
23. A. N. Glazer, *Method. Enzymol.*, 1988, **167**, 291-303.
24. C. L. Mulder, L. Theogarajan, M. Currie, J. K. Mapel, M. A. Baldo, M. Vaughn, P. Willard, B. D. Bruce, M. W. Moss, C. E. McLain and J. P. Morseman, *Adv. Mater.*, 2009, **21**, 3181-3185.
25. R. Bose, M. Gonzalez, P. Jenkins, R. Walters, J. Morseman, M. Moss, C. McLain, P. Linsert, A. Buchtemann, A. J. Chatten and K. W. J. Barnham, presented in part at the 35th IEEE Photovoltaic Specialists Conference, Honolulu, USA, 20-25 June, 2010.
26. A. R. Frias, S. F. H. Correia, M. Martins, S. P. M. Ventura, E. Pecoraro, S. L. Ribeiro, P. S. Andre, R. A. S. Ferreira, J. A. P. Coutinho and L. D. Carlos, *Adv. Sustain. Syst.*, 2019, **3**, 1800134.
27. J. C. White and L. Stryer, *Anal. Biochem.*, 1987, **161**, 442-452.
28. A. Gaigalas, T. Gallagher, K. D. Cole, T. Singh, L. L. Wang and Y. Z. Zhang, *Photochem. Photobiol.*, 2006, **82**, 635-644.
29. S. H. Park and R. T. Raines, *Protein Sci.*, 1997, **6**, 2344-2349.
30. R. Zhuang, Y. Zhang, R. Zhang, C. Song, K. Yang, A. Yang and B. Jin, *Protein Expression Purif.*, 2008, **59**, 138-143.
31. A. V. Yakhnin, L. M. Vinokurov, A. K. Surin and Y. B. Alakhov, *Protein Expression Purif.*, 1998, **14**, 382-386.
32. O. J. Stone, K. M. Biette and P. J. M. Murphy, *PLoS One*, 2014, **9**, e108611.
33. M. M. Nalaskowski, P. Ehm, S. Giehler and G. W. Mayr, *Anal. Biochem.*, 2012, **428**, 24-27.
34. J. R. Deschamps, C. E. Miller and K. B. Ward, *Protein Expression and Purif.*, 1995, **6**, 555-558.
35. M. Martins, C. W. Ooi, M. C. Neves, J. F. B. Pereira, J. A. P. Coutinho and S. P. M. Ventura, *J. Chem. Technol. Biot.*, 2018, **93**, 1864-1870.
36. M. Zimmer, *Chem. Rev.*, 2002, **102**, 759-781.
37. M. Munier, S. Jubeau, A. Wijaya, M. Morancais, J. Dumay, L. Marchal, P. Jaouen and J. Fleurence, *Food Chem.*, 2014, **150**, 400-407.
38. A. B. Cubitt, L. A. Woollenweber and R. Heim, in *Methods in Cell Biology*, ed. K. F. Sullivan and S. A. Kay, Elsevier Inc., 1998, vol. 58, ch. 2, 19-30.
39. S. Veettil, N. Budisa and G. Jung, *Biophys. Chem.*, 2008, **136**, 38-43.
40. R. Heim and R. Y. Tsien, *Curr. Biol.*, 1996, **6**, 178-182.
41. M. Bottrill and M. Green, *Chem. Commun.*, 2011, **47**, 7039-7050.
42. R. Hardman, *Environ. Health Persp.*, 2006, **114**, 165-172.
43. N. V. dos Santos, M. Martins, V. C. Santos-Ebinuma, S. P. M. Ventura, J. A. P. Coutinho, S. R. Valentini and J. F. B. Pereira, *ACS Sustain. Chem. Eng.*, 2018, **6**, 9383-9393.
44. R. Reisfeld, D. Shamrakov and C. Jorgensen, *Sol. Energ. Mat. Sol. C*, 1994, **33**, 417-427.
45. S. F. H. Correia, P. P. Lima, P. S. Andre, R. A. S. Ferreira and L. D. Carlos, *Sol. Energ. Mat. Sol. C.*, 2015, **138**, 51-57.
46. R. Heim, D. C. Prasher and R. Y. Tsien, *P. Natl. Acad Sci. USA*, 1994, **91**, 12501-12504.
47. R. Y. Tsien, *Annu. Rev. Biochem.*, 1998, **67**, 509-544.
48. T. M. H. Creemers, A. J. Lock, V. Subramaniam, T. M. Jovin and S. Volker, *Nat. Struct. Biol.*, 1999, **6**, 557-560.
49. M. Cotlet, J. Hofkens, M. Maus, T. Gensch, M. Van der Auweraer, J. Michiels, G. Dirix, M. Van Guyse, J. Vanderleyden, A. J. W. G. Visser and F. C. De Schryver, *J. Phys. Chem. B*, 2001, **105**, 4999-5006.
50. K. D. Piatkevich, V. N. Malashkevich, K. S. Morozova, N. A. Nemkovich, S. C. Almo and V. V. Verkhusha, *Sci. Rep. - UK*, 2013, **3**, 1847.
51. L. D. Carlos, V. de Zea Bermudez, R. A. S. Ferreira, L. Marques and M. Assunção, *Chem. Mater.*, 1999, **11**, 581-588.
52. L. D. Carlos, R. A. S. Ferreira, V. de Zea Bermudez and S. J. L. Ribeiro, *Adv. Funct. Mater.*, 2001, **11**, 111-115.
53. L. D. Carlos, R. A. S. Ferreira, R. N. Pereira, M. Assunção and V. de Zea Bermudez, *J. Phys. Chem. B*, 2004, **108**, 14924-14932.
54. S. S. Nobre, P. P. Lima, L. Mafra, R. A. S. Ferreira, R. O.

View Article Online
DOI: 10.1039/D0GC01742F

Freire, L. S. Fu, U. Pischel, V. de Zea Bermudez, O. L. Malta and L. D. Carlos, *J. Phys. Chem. C*, 2007, **111**, 3275-3284.
55. R. A. S. Ferreira, L. D. Carlos, R. R. Goncalves, S. J. L. Ribeiro and V. D. Bermudez, *Chem. Mater.*, 2001, **13**, 2991-2998.
56. R. A. S. Ferreira, M. Nolasco, A. C. Roma, R. L. Longo, O. L. Malta and L. D. Carlos, *Chem. Eur. J.*, 2012, **18**, 12130-12139.
57. K. Suhling, J. Siegel, D. Phillips, P. M. W. French, S. Leveque-Fort, S. E. D. Webb and D. M. Davis, *Biophys. J.*, 2002, **83**, 3589-3595.
58. H. Morise, O. Shimomura, F. H. Johnson and J. Winant, *Biochemistry*, 1974, **13**, 2656-2662.
59. M. Chalfie, *Photochem. Photobiol.*, 1995, **62**, 651-656.
60. P. Reineck, A. Francis, A. Orth, D. W. M. Lau, R. D. V. Nixon-Luke, I. Das Rastogi, W. A. W. Razali, N. M. Cordina, L. M. Parker, V. K. A. Sreenivasan, L. J. Brown and B. C. Gibson, *Adv. Opt. Mater.*, 2016, **4**, 1549-1557.
61. R. Rondão, A. R. Frias, S. F. H. Correia, L. S. Fu, V. de Zea Bermudez, P. S. André, R. A. S. Ferreira and L. D. Carlos, *ACS Appl. Mater. Interfaces*, 2017, **9**, 12540-12546.
62. K. F. Wu, H. B. Li and V. I. Klimov, *Nat. Photonics*, 2018, **12**, 105-110.
63. V. I. Klimov, T. A. Baker, J. Lim, K. A. Velizhanin and H. McDaniel, *ACS Photonics*, 2016, **3**, 1138-1148.
64. V. Sholin, J. D. Olson and S. A. Carter, *J. Appl. Phys.*, 2007, **101**, 123114.
65. X. Liu, B. Luo, J. Liu, D. Jing, D. Benetti and F. Rosei, *J. Mater. Chem. A*, 2020, **8**, 1787-1798.
66. G. V. Shcherbatyuk, R. H. Inman, C. Wang, R. Winston and S. Ghosh, *Appl. Phys. Lett.*, 2010, **96**, 191901.
67. A. L. Rodarte, F. Cisneros, L. S. Hirst and S. Ghosh, *Liq. Cryst.*, 2014, **41**, 1442-1447.
68. Z. Krumer, W. G. J. H. M. van Sark, R. E. I. Schropp and C. D. Donega, *Sol. Energ. Mat. Sol. C.*, 2017, **167**, 133-139.
69. A. F. Mansour, *Polym. Test.*, 1998, **17**, 153-162.
70. J. A. H. P. Sol, V. Dehm, R. Hecht, F. Würthner, A. P. H. J. Schenning and M. G. Debije, *Angew. Chem. Int. Ed.*, 2017, **56**, 1-5.